

# Direct observation of the sub-Doppler trap in a parametrically driven magneto-optical trap

Kihwan Kim,<sup>1</sup> Heung-Ryoul Noh,<sup>2,\*</sup> Hyun-Ji Ha,<sup>1</sup> and Wonho Jhe<sup>1</sup>

<sup>1</sup>*School of Physics and Center for Near-field Atom-photon Technology, Seoul National University, Seoul 151-742, Korea*

<sup>2</sup>*Department of Physics, Chonnam National University, Gwangju 500-757, Korea*

(Received 14 September 2003; published 17 March 2004)

The double structure potential predicted in the atomic cloud of a magneto-optical trap by one- (Doppler part) and two-photon process (sub-Doppler part) is experimentally observed and studied through the parametric excitation with the modulation of cooling laser intensities. Modulating the intensity of the cooling laser at around twice its resonant frequency of Doppler part, the atoms in Doppler part are divided and they oscillate reciprocally with finite amplitude due to the nonlinearity of the trap, and the others in sub-Doppler part are not influenced. By the modulation, we can investigate the sub-Doppler part spatially without Doppler part and also measure the temperature of sub-Doppler part independently.

DOI: 10.1103/PhysRevA.69.033406

PACS number(s): 32.80.Pj, 05.45.-a

## I. INTRODUCTION

Nowadays a magneto-optical trap (MOT) [1] is one of the worldwide basic tools to study the atomic properties, and is applied to a large number of experiments of atomic physics and atom optics field, such as atomic beam, Bose-Einstein condensations, atomic clock, atom lithography, and atom interferometry [2]. Many properties of MOT such as lower temperature and larger cloud size than Doppler limit were well understood by the polarization gradient cooling [3] and radiation trapping [4,5], respectively. Concerning the question of the structure in a MOT, however, there have been qualitative discussions [5,6] on the basis of polarization gradient cooling. In recent years the authors in Ref. [7] calculated and showed that the potential well of the MOT has double-component structure, that is, there is a sharp bottom part (sub-Doppler part) resulting from the two-photon process near the center of the potential of radiation pressure force due to one-photon process (Doppler part). Even though many experiments about the shapes and structures of the MOT have been performed [4,8,9], that kind of double structure was experimentally observed just indirectly as its influence on the atomic density distribution [10]. Moreover, there has been nearly no experimental study about the double structure of the MOT in a systematic and quantitative manner.

In this paper we report the direct observation of sub-Doppler part of the MOT through the parametric resonance which was achieved by the modulation of cooling laser intensities, and confirm the double structure of the MOT experimentally. We also investigated experimentally the properties of Doppler and sub-Doppler part of the MOT such as the spatial profile, the temperature, and the number density, and showed that these observations are in well agreement with the calculation in Ref. [7].

## II. EXPERIMENTAL OBSERVATIONS: PARAMETRIC RESONANCE OF THE MOT

Recently we have studied a parametric resonance in a MOT: when the intensities of the cooling lasers are modu-

lated at about twice its natural frequencies, the atoms in the MOT are divided into two parts and they oscillate reciprocally with finite amplitude due to nonlinearity of the trap [11]. Based on the simple Doppler cooling theory, we have explained the observations of limit cycles, and subcritical and supercritical Hopf bifurcations. By appropriate choice of experimental parameters, the motions along the  $z$  axis (anti-Helmholtz coils) are parametrically excited.

Assuming that the counterpropagating laser intensities are modulated with  $I(1 + \varepsilon \cos \omega t)$ , where  $I$  is the intensity of a laser beam,  $\varepsilon$  and  $\omega$  are the modulation amplitude and frequency, respectively, the one-dimensional equation of motion for a two-level atom in a MOT is given by

$$m\ddot{z} = F_{\text{Dop}}(z, v, t), \quad (1)$$

where the Doppler force is simply given by

$$F_{\text{Dop}}(z, v, t) = \frac{\hbar k \Gamma}{2} \left( \frac{s(t)}{1 + s(t) + 4 \left[ \frac{\delta}{\Gamma} - \frac{k}{\Gamma} v - \frac{\mu_B b}{\hbar \Gamma} z \right]^2} - \frac{s(t)}{1 + s(t) + 4 \left[ \frac{\delta}{\Gamma} + \frac{k}{\Gamma} v + \frac{\mu_B b}{\hbar \Gamma} z \right]^2} \right). \quad (2)$$

Here  $k$  is the wave number,  $\mu_B$  is Bohr magneton,  $\Gamma$  is the natural linewidth,  $m$  is the atomic mass,  $b$  is the magnetic-field gradient,  $\delta$  is the detuning of the laser frequency  $\omega_L$  with respect to the atomic resonance  $\omega_A$  ( $\delta = \omega_L - \omega_A$ ), and  $s(t) = s_0(1 + \varepsilon \cos \omega t)$  with the normalized laser intensity  $s_0$  ( $= I/I_s$ , with  $I_s$  being the saturation intensity, 1.62 mW/cm<sup>2</sup> for the  $D_2$  line of <sup>85</sup>Rb atoms).

When we expand Eq. (1) up to the first order in  $z$  or  $\dot{z}$ , it becomes a typical Mathieu equation and can be given by [12]

$$\ddot{z} + \beta_{\text{Dop}} \dot{z} + \omega_{\text{Dop}}^2 (1 + \varepsilon \cos \omega t) z = 0, \quad (3)$$

where the natural frequency is

\*Corresponding author. Email address: hrnoh@chonnam.ac.kr

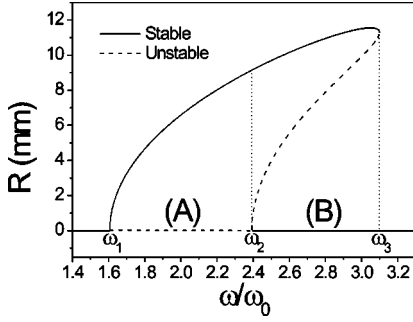


FIG. 1. The calculated amplitude of a limit cycle. The parameters are as follows:  $s_0=0.05$ ,  $b=9$  G/cm,  $\varepsilon=0.9$ , and  $\delta/\Gamma=-2.9$ .

$$\omega_{\text{Dop}} = \sqrt{\frac{8\mu_B b k s_0 |\delta/\Gamma|}{m[1 + 4(\delta/\Gamma)^2]^2}}, \quad (4)$$

with the damping coefficient  $\beta_{\text{Dop}} = (\hbar k / \mu_B b) \omega_{\text{Dop}}^2$ . To excite the parametric resonance, we can vary the parameters such as the magnetic field gradient  $b$ , the detuning  $\delta$ , or the normalized laser intensity  $s_0$ .

With appropriate experimental conditions, the atomic motion exhibits a limit cycle motion, which can be approximately expressed by  $z(t) = R \cos(\omega t/2 + \phi)$ , where  $R$  is the amplitude and  $\phi$  is the phase of the limit cycle motion [13]. Figure 1 shows the typical solutions of the amplitude for Eq. (1) with the parameters used in the experiment. In the figure the solid (dashed) line denotes the stable (unstable) solutions. For a given  $R$ , there exist two values of  $\phi$  with the difference of  $\pi$ , resulting from the fact that the system has odd spatial symmetry. The limit cycle motions are excited when the modulation amplitude exceeds a threshold value ( $\varepsilon_T = 2\beta_{\text{Dop}}/\omega_{\text{Dop}}$ ). The upper limit of the saturation parameter results from the condition  $\varepsilon_T < 1$ , and is given by

$$s_0 < \frac{m\mu_B b [1 + 4(\delta/\Gamma)^2]^2}{32\hbar^2 k^3 (-\delta/\Gamma)}. \quad (5)$$

In Fig. 1 the characteristic frequencies up to the first order in  $\varepsilon$  are presented, and are given by  $\omega_1 = 2\omega_0 - (\omega_0/2)\sqrt{\varepsilon^2 - \varepsilon_T^2}$ ,  $\omega_2 = 2\omega_0 + (\omega_0/2)\sqrt{\varepsilon^2 - \varepsilon_T^2}$ , and  $\omega_3 = \omega_0 + (\varepsilon\omega_0/2\varepsilon_T)\sqrt{4 + \varepsilon_T^2}$ . There exists a trivial solution  $R=0$ , which is unstable at the frequency region A ( $\omega_1 < \omega < \omega_2$ ) and stable at other frequency regions. We have two stable (nontrivial) solutions and one unstable (trivial) solution for region A ( $\omega_1 < \omega < \omega_2$ ), while three stable (two nontrivial and one trivial) solutions and two unstable solutions for region B ( $\omega_2 < \omega < \omega_3$ ). In the previous work the supercritical and subcritical Hopf bifurcation have been reported [11].

The experimental procedures are well described in the previous reports [11]. Typical experimental parameters are as follows: in the  $z$  axis,  $s_0=0.05$ ,  $b=9$  G/cm, the amplitude of modulation  $\varepsilon=0.9$ , and  $\delta/\Gamma=-2.9$ . Thus  $\omega_{\text{Dop}}$  is about  $2\pi \times 34.3$  Hz and  $\omega_{\text{sub}}$  (will be explained in the following section) is  $2\pi \times 460$  Hz. Since the saturation parameters in the transverse directions ( $s_x=s_y=0.25$ ) are larger than the upper limit ( $=0.13$ ) given in Eq. (5), the parametric resonance occurs only in the  $z$  axis. The full width of MOT beams at the

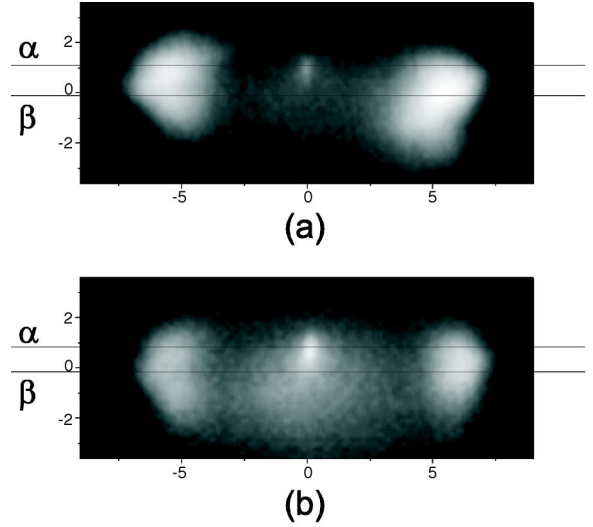


FIG. 2. The typical appearance of (a) double and (b) triple fixed points in experiments. The modulation frequency is 80 Hz (a) and 95 Hz (b). The profiles of (a)[(b)] along  $\alpha$  and  $\beta$  lines are presented in Fig. 4 (Fig. 5).

$e^{-1/2}$  intensity point is 2.5 cm in order to cover the whole range of atomic motion ( $2R$ ). The total number of atoms in the unmodulated MOT is about  $2 \times 10^8$  and that in the modulated MOT is about  $8 \times 10^7$ . Figure 2 shows the photos of parametrically excited atoms at the modulation frequency of 80 Hz (a) and 95 Hz (b). Both frequencies belong to regions A and B in Fig. 1, respectively. They are taken from a charge-coupled device camera with  $1/2400$  s of exposure time at the 0 degree phase with respect to the modulated laser intensity.

In Fig. 2(a), according to the Doppler theory explained above, the modulation frequency belongs to region A in Fig. 1. Although in that region we have to see two atomic clouds from limit cycle motions, we have observed another atomic cloud at the origin of magnetic field. With the only scope of Doppler theory this kind of central cloud could not be understood. Moreover, the characteristics of the cloud are much different from those of the third fixed point in region B of Fig. 1. The size and width of the central cloud in Fig. 2(a) is much smaller and narrower. In Fig. 2(b), the middle cloud shows double structure which is composed of relatively large and broad cloud, and small and narrow one. We can easily notice that the broad and large trap in Fig. 2(b) is fundamentally attributable to the third fixed point at the origin of the magnetic field with the Doppler theory. On the other hand, the narrow and sharp traps in Figs. 2(a) and 2(b) have a different origin, which can be very well understood by including the sub-Doppler cooling theory [7]. Here we have to note the phase at which the images are taken. Even though the widths of the atomic clouds are varied at different phases, the important characters of which we will make detailed investigations are not influenced by them. We think that the one image taken at the specific phase is sufficient to study the sub-Doppler characters of MOT.

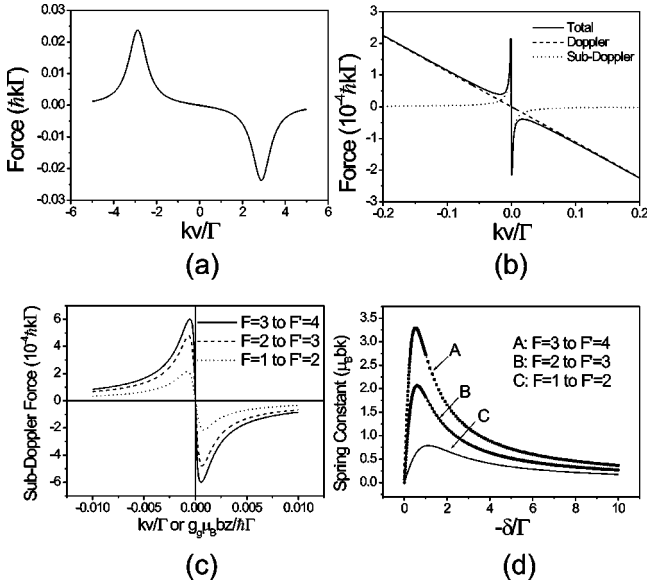


FIG. 3. The calculated total force in the enlarged (a) and detailed region (b). (c) The sub-Doppler force for various transition lines. (d) The calculated spring constant ( $m\omega_{\text{sub}}^2$ ) for various transition lines as functions of detuning.

### III. DOUBLE STRUCTURE POTENTIAL IN THE MOT

In order to comprehend the trap, it is necessary to consider the sub-Doppler laser cooling theory, which explains the abnormal low temperature in the optical molasses or in a MOT. By the calculation of authors of Ref. [7] there exist two kinds of traps in a normal MOT: One is due to one-photon process, that is, Doppler cooling theory, and the other is due to two-photon process, which makes sub-Doppler temperature. Thus the force exerted on an atom is given by

$$F(z, v, t) = F_{\text{Dop}}(z, v, t) + F_{\text{sub}}(z, v, t), \quad (6)$$

where the Doppler force [ $F_{\text{Dop}}(z, v, t)$ ] is given in Eq. (2) and the sub-Doppler force for a  $F=1 \rightarrow F'=2$  atomic transition line is analytically given by [7]

$$F_{\text{sub}}(z, v, t) = f\left(\frac{kv}{\Gamma} + \frac{g_g \mu_B b z}{\hbar \Gamma}\right). \quad (7)$$

Here the function  $f(x)$  is given by

$$f(x) = -\frac{120\hbar k \Gamma s(t)^2 |\delta \Gamma| x}{17s(t)^2 [5 + 4(\delta \Gamma)^2] + 2112[1 + 4(\delta \Gamma)^2]^2 x^2}, \quad (8)$$

with  $g_g$  as the  $g$  factor of the ground state and  $s(t) = s_0(1 + \varepsilon \cos \omega t)$  the normalized modulated laser intensity. Now let us assume the unmodulated laser intensity, that is,  $s(t) = s_0$ . After we calculate the force with  $s_0$ , we merely replace  $s_0$  with  $s(t)$ . Figure 3(a) shows the typical calculation of the total force and Fig. 3(b) shows the same force for the detailed region for  $F=1 \rightarrow F'=2$  atomic transition line. We can see that the sub-Doppler force exists only near the origin. The sub-Doppler force for other transition lines can be calculated numerically as shown in Fig. 3(c)

[14]. For  $F=1 \rightarrow F'=2$  level scheme, since it has equal  $g$  factors for ground and excited states, the sub-Doppler force is completely described by Eq. (7), where the steep slope always crosses the  $z$  or  $v$  axis. For other level schemes, however, the difference of the  $g$  factors leads to the displacement of the sub-Doppler force. Thus the sharp slope does not cross the  $z(v)$  axis for large  $z(v)$ . As a result, the force is not completely described by Eq. (7) for other level schemes. However, in the vicinity of the origin, i.e.,  $z \approx 0$  and  $v \approx 0$ , we can approximately use Eq. (7) with different coefficients which depend on the detuning and the laser intensity. Since the quantitative explanation is not our main aim, although our scheme is  $F=3 \rightarrow F'=4$ , we use Eq. (7) with the  $g_g = 1/3$  for a  $^{85}\text{Rb}$  atom.

The trap frequency can be derived from Eq. (7) as

$$\omega_{\text{sub}} = \sqrt{\frac{P_1 \mu_B b k |\delta \Gamma|}{m[1 + P_2 (\delta \Gamma)^2]}}, \quad (9)$$

with the coefficients  $P_1 = 24/17$  and  $P_2 = 4/5$  for a  $F=1 \rightarrow F'=2$  atomic transition line, and is plotted in Fig. 3(d) (C) as a function of the detuning. The trap frequencies for other transition lines can be calculated numerically, and are shown in Fig. 3(d) (A and B), where the points describe the calculated spring constants and the lines are the fitted results with Eq. (9). The coefficients obtained with the data fitting are  $P_1 = 6.84$  and  $P_2 = 2.72$  for  $F=2 \rightarrow F'=3$  transition, and  $P_1 = 12.5$  and  $P_2 = 3.57$  for  $F=3 \rightarrow F'=4$  transition. Comparing Eqs. (4) and (9), it is easily seen that the trap frequency of sub-Doppler MOT has no laser intensity dependence, while the trap frequency of Doppler MOT is proportional to  $\sqrt{s_0}$ , which gives rise to parametric resonance. Note that, since the frequency is independent of the intensity, the parametric resonance cannot be excited through the intensity modulation. Accordingly, we can selectively excite parametric resonance for the Doppler part, and observe the sub-Doppler MOT alone without the Doppler MOT. It is also confirmed that the trap frequency does not depend on the laser intensity from the calculation. Since the frequency in Eq. (9) is proportional to  $\sqrt{b}$ , it seems that the parametric resonance can be excited by the modulation of the magnetic-field gradient. However, in our experimental conditions, the magnetic-field gradient should be larger than 4000 G/cm to fulfill the condition  $\varepsilon_T < 1$ , which is unrealistic. Thus we can conclude that the sub-Doppler MOT cannot be excited by the modulation of the magnetic-field gradient.

### IV. SIMULATION RESULTS AND CONCLUSIONS

We compare the profiles of Fig. 2 with the Monte Carlo simulations with and without considering the sub-Doppler force. One can obviously see that the experimental profiles and the simulations are in excellent agreement. Figure 4(a) is the profile of Fig. 2(a) along the  $\alpha$  line and Fig. 4(b) is that of Fig. 2(a) along the  $\beta$  line. The profiles of Fig. 2(b) along the  $\alpha$  line and the  $\beta$  line are shown in Figs. 5(a) and 5(b), respectively. In the figures the left one is the experimental data and the right one is the simulation result. While the

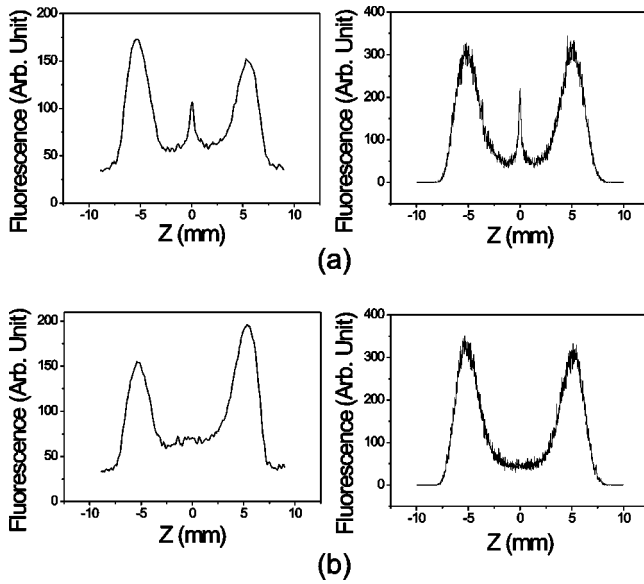


FIG. 4. (a) [(b)] is the profile of Fig. 2(a) along the  $\alpha$  ( $\beta$ ) line. In (a) and (b), the left one is the measured profile and the right one is the simulation result.

calculations are purely one dimensional, the experimental situations are three dimensional. In the experiments, because of very small size of the sub-Doppler trap, the profiles of Fig. 2 could show different natures. That is, the profile of the  $\alpha$  line which goes through the sub-Doppler trap exhibits the effect of sub-Doppler trap force, while that of the  $\beta$  line which goes out of sub-Doppler trap is nearly the same as the result of simulations without sub-Doppler force. Note that the slight displacement of the center of the sub-Doppler trap from that of the Doppler trap in Fig. 2 must be due to the laser intensity imbalance, which comes from the retroreflecting geometry of lasers along the  $x$  or  $y$  axis.

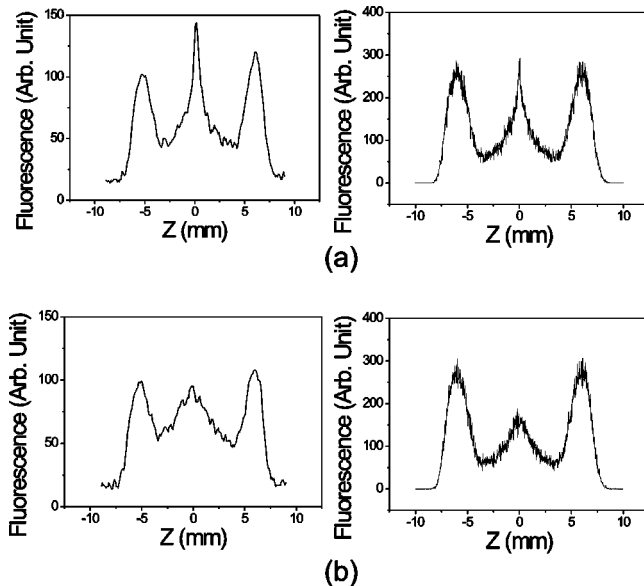


FIG. 5. (a) [(b)] is the profile of Fig. 2(b) along the  $\alpha$  ( $\beta$ ) line. In (a) and (b), the left one is the measured profile and the right one is the simulation result.

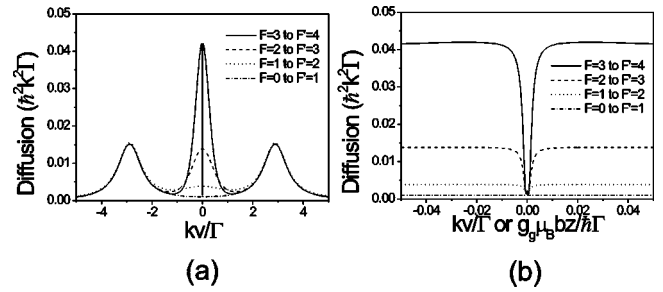


FIG. 6. (a) The calculated momentum diffusion coefficients for various atomic transition lines. (b) The detailed plots near the origin.

Figures 4(a) and 5(a) are obtained from the Monte Carlo simulations by taking into account the sub-Doppler laser cooling theory as explained above. We have used the combined force [Eq. (6)] in the simulation. In the meanwhile, Figs. 4(b) and 5(b) are obtained by only taking into account the Doppler force. In addition, we also take into consideration the random recoil force  $f_r$  from the spontaneously emitted photons. The random force is related with the momentum diffusion via the following equation:

$$\langle f_r(t)f_r(t') \rangle = 2D_{zz}(t)\delta(t-t'), \quad (10)$$

where  $D_{zz}(t)$  is the momentum diffusion coefficient for  $z$  axis and the left-hand side of Eq. (10) denotes the average of product of the force at the different time over long time.

The momentum diffusion coefficients for various transition lines are presented in Fig. 6(a) [14], where we have assumed the unmodulated laser intensity, i.e.,  $s(t)=s_0$ . In Fig. 6(a) the result for  $F=0 \rightarrow F'=1$  corresponds to that of Doppler theory. The calculated results for the detailed region are shown in Fig. 6(b). Near the center of the velocity, there exists a sharp dip, which exhibits the feature of two-photon resonance, that is, sub-Doppler laser cooling theory. We can see that the magnitude of the diffusion coefficient increases with the increasing angular momentum of the ground state. In the simulation we have used the calculated momentum diffusion coefficient in the sub-Doppler cooling theory for  $F=3 \rightarrow F'=4$  transition line.

The diffusion coefficient is very important to determine the widths of the atomic clouds. With only the diffusion coefficient from Doppler theory which is much smaller than that from sub-Doppler theory near the center of the velocity or position, there is very big discrepancy between the experimental results and the calculations by about five times. The widths of the trapped clouds are very sensitive to the amount of momentum diffusion and are influenced by other origins such as the reabsorptions of the photons emitted by the nearby atoms and the shadow effect which is important when the number of atoms in cloud is large. As a result, it is very difficult to exactly calculate the width in the simulation. In our scheme, when we adopt the sub-Doppler momentum diffusion coefficient, although we only take into account the one-dimensional motion and also neglect all other effects which may contribute to the determination of the width, we can obtain similar results as in the experiment.

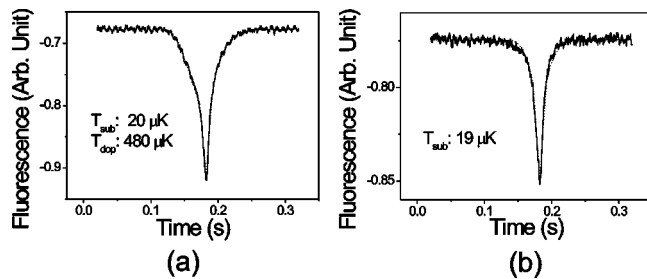


FIG. 7. (a) The fluorescence signal of the ordinary MOT by a TOF method. We can see clearly the double structure of the TOF signal, which is combined by the Doppler trap and sub-Doppler trap. The temperature of the Doppler trap is around  $480 \mu\text{K}$ , while that of the sub-Doppler trap is  $20 \mu\text{K}$ . (b) is the TOF signal which is obtained after the modulation of the cooling laser.

In Fig. 4, the experimental (simulation) result of width (twice the standard deviation in the Gaussian distribution) of broad peaks is approximately  $2.1 \text{ mm}$  ( $2.2 \text{ mm}$ ). Also the experimental (simulation) width of central peak is  $0.45 \text{ mm}$  ( $0.28 \text{ mm}$ ). In Fig. 5, the experimental (simulation) width of oscillating broad peak, central broad peak, and the central sharp peak is  $1.7$  ( $1.9 \text{ mm}$ ),  $5.6$  ( $5.2 \text{ mm}$ ), and  $0.68$  ( $0.26 \text{ mm}$ ), respectively. We can see the good agreements between the experimental and simulation results.

We also measure the temperature of the sub-Doppler trap without Doppler trap. Our experimental situation of measuring the temperature is described in Ref. [15]. Figure 7(a) shows the fluorescence signal of ordinary MOT by a time-of-flight (TOF) method. From Fig. 7(a) we can clearly see the double structure of TOF signal, which is combined by Doppler trap and sub-Doppler trap. In this case the temperature of Doppler trap is around  $480 \mu\text{K}$ , while that of sub-Doppler trap is  $20 \mu\text{K}$ . Figure 7(b) is the TOF signal which is obtained after the modulation of cooling laser, and shows the temperature of  $19 \mu\text{K}$ . We turn off the cooling laser to

detect the TOF at the time that the Doppler traps divided have so large velocity that the Doppler part of MOT does not contribute to the TOF signal. In Fig. 7(b) the number of atoms in Doppler part reduces by 40 times, and we can see the TOF of atoms in sub-Doppler part. The number of atoms trapped in sub-Doppler MOT is  $3.2 \times 10^6$ , the full width at half maximum is  $0.6 \text{ mm}$  (since the temperature-measurement experiment was carried out separately with the values in Fig. 4 or Fig. 5), the number density is  $8 \times 10^{10} \text{ cm}^{-3}$ , and the phase-space density is  $6 \times 10^{-6}$ , which is larger than the typical MOT. However, it is a little bit smaller than the values reported in typical sub-Doppler MOT [5]. We should comment on the reason why this sub-Doppler part was not shown in Fig. 2(a) of Ref. [11]. The main difference between the previous experiment and the current one is the average intensity of cooling laser. When the intensity of cooling laser is lower than a certain value, the trap width of sub-Doppler part is so small that the atoms do not form the sub-Doppler trap.

In conclusion, we directly observe the sub-Doppler part of the MOT without the Doppler part by using the parametric resonance which is achieved by the modulation of the intensity of cooling lasers. We compare the spatial profile of sub-Doppler trap with the Monte Carlo simulation, and observe they are in good agreement. The temperature of sub-Doppler part without Doppler part is also measured by TOF, which confirms that the small localized trap during the intensity modulation should be the sub-Doppler trap.

#### ACKNOWLEDGMENTS

This work was supported by the Creative Research Initiative Project of the Korea Ministry of Science and Technology. H.R.N. was supported by a Korea Research Foundation grant (Grant No. KRF-2003-003-C00057).

- 
- [1] E. L. Raab, M. Prentiss, A. Cable, S. Chu, and D. E. Pritchard, *Phys. Rev. Lett.* **59**, 2631 (1987).
- [2] H. J. Metcalf and P. van der Straten, *Laser Cooling and Trapping* (Springer, New York, 1999).
- [3] J. Dalibard and C. Cohen-Tannoudji, *J. Opt. Soc. Am. B* **6**, 2023 (1989).
- [4] T. Walker, D. Sesko, and C. Wieman, *Phys. Rev. Lett.* **64**, 408 (1990); D. W. Sesko, T. G. Walker, and C. E. Wieman, *J. Opt. Soc. Am. B* **8**, 946 (1991).
- [5] C. G. Townsend, N. H. Edwards, C. J. Cooper, K. P. Zetie, C. J. Foot, A. M. Steane, P. Szriftgiser, H. Perrin, and J. Dalibard, *Phys. Rev. A* **52**, 1423 (1995).
- [6] A. M. Steane, M. Chowdhury, and C. J. Foot, *J. Opt. Soc. Am. B* **9**, 2142 (1992).
- [7] J. W. Jun, S. Chang, T. Y. Kwon, H. S. Lee, and V. G. Minogin, *Phys. Rev. A* **60**, 3960 (1999); J. W. Jun, S. Chang, H. S. Lee, V. Minogin, and W. Jhe, *ibid.* **60**, 4738 (1999); S. Chang and V. Minogin, *Phys. Rep.* **365**, 65 (2002).
- [8] I. Guedes, M. T. de Araujo, D. M. B. P. Milori, G. I. Surdovich, V. S. Bagnato, and S. C. Zilio, *J. Opt. Soc. Am. B* **11**, 1935 (1994); V. S. Bagnato, L. G. Marcassa, M. Oria, G. I. Surdovich, R. Vitlina, and S. C. Zilio, *Phys. Rev. A* **48**, 3771 (1993).
- [9] M. Drewsen, Ph. Laurent, A. Nadir, G. Santarelli, A. Clairon, Y. Castin, D. Grinson, and C. Salomon, *Appl. Phys. B: Lasers Opt.* **B59**, 283 (1994).
- [10] W. Petrich, M. H. Anderson, J. R. Ensher, and E. A. Cornell, *J. Opt. Soc. Am. B* **11**, 1332 (1994).
- [11] K. Kim, H. R. Noh, Y. H. Yeon, and W. Jhe, *Phys. Rev. A* **68**, 031403 (2003).
- [12] L. D. Landau and E. M. Lifshitz, *Mechanics* (Pergamon, London, 1976).
- [13] S. H. Strogatz, *Nonlinear Dynamics and Chaos* (Perseus, New York, 2001).
- [14] M. Walhout, J. Dalibard, S. L. Rolston, and W. D. Phillips, *J. Opt. Soc. Am. B* **9**, 1997 (1992).
- [15] K. Kim, H. R. Noh, Y. H. Yeon, V. G. Minogin, and W. Jhe, *Phys. Rev. A* **65**, 055404 (2002).